Re-entry trajectory optimization for a SSTO vehicle in the presence of atmospheric uncertainties

Fabrizio Pescetelli and Edmondo Minisci and Richard E Brown
Centre for Future Air-Space Transportation Technology,
Dept. of Mechanical and Aerospace Engineering
University of Strathclyde, Glasgow G4 0LT, Scotland, UK

Abstract

This paper addresses the design of the unpowered re-entry trajectory of a fully reusable, winged, unmanned single-stage-to-orbit (SSTO) vehicle, as the last phase of a payload deployment into low Earth orbit. A hybrid optimisation technique that couples a population-based, stochastic algorithm with a deterministic, gradient-based technique is used to minimize the heat load along the re-entry trajectory after accounting for operational constraints on the heat flux and normal acceleration. Uncertainties in the atmospheric model are considered to evaluate their effects on the vehicle performance. Firstly, the deterministic optimal control law is re-integrated after introducing uncertainties into the model. The proximity of the final solutions to the target states are analysed statistically. A second analysis is then performed, aimed at determining the best performance of the vehicle when these uncertainties are included directly in the optimisation. The statistical analysis of the results so obtained are summarized by an expectancy curve which represents the probable vehicle performance as a function of the uncertain system parameters. This analysis can be used during the preliminary phase of design to yield valuable insights into the robustness of the performance of the vehicle to uncertainties in the specification of its parameters.

1. Introduction

Although launch vehicles are indispensable in space exploration and transportation, the current expendable launch systems represent an expensive way to get access to space. To reduce its cost, the technology to design new space-to-access vehicles is currently an active field of research. By emphasizing on full re-usability in their design and employing an airline-like approach, where the costs of development are amortized over repeated flights, these vehicles promise to dramatically reduce the cost per kilogram of access to space. In the process of designing the next generation of reusable launchers, it is fundamental that safety and reliability in trajectory planning are obtained. During re-entry, the intense heating environment to which the vehicle is exposed is one of the most challenging problems to overcome. In fact, the control has to steer the re-entry corridor on feasible trajectories constrained by deceleration and heating. The overarching aim of the research described in this paper is to develop a model-based software tool that will aid in the preliminary design of the next generation of space-access vehicles. A winged re-usable single-stage-to-orbit (SSTO) vehicle is designed to perform a full mission, based on an ascent trajectory, low orbit for payload delivering, and re-entry phase. Within this paper the unpowered re-entry trajectory of a SSTO is designed by optimising a control law that alters the angle of attack and the bank angle of the vehicle along its trajectory to the TAEM point [1]. In the process of preliminary design, it is fundamental that any new tools and approaches that are developed for the evaluation of vehicle performance are also capable of functioning reliably in an integrated design environment. As such, the optimal trajectories that result from application of these tools need to be robust, as they have to consider of the effect of uncertainties within the various parameters and models that comprise the overall vehicle system design. During the process whereby the control law is optimized in order to minimize the total heat load at the TAEM interface, it is thus also highly desirable to be able to assess the sensitivity of the design to variations, for instance, on atmospheric data which influence the heating model prediction and aerodynamics. In addition to finding a representative control law for the re-entry trajectory of a spaceplane, the uncertainties in the atmospheric model which characterize the tool are included in order to estimate their impact on the overall vehicle performance. Two analyses are performed. In the first analysis, a set of trajectories which use the nominal optimal control law is integrated implementing the uncertainty within the atmospheric model. With the second analysis the control law is re-optimised and the uncertainties are included within

the optimization loop to determine their effect on the vehicle performance. A statistical analysis is conducted on the results in order to produce an expectancy curve which relates the probability of the vehicle having a certain performance to the expected variation due to uncertainty in the system design parameters. The optimization process proposed here is based on a hybrid stochastic-deterministic algorithm which combines a global explorative search and a local search. This approach is revealed to overcome successfully the limitations of gradient-based solvers, as they are affected by the presence of discontinuities in any system models and this makes it difficult to find an optimal solution if a good initial guess is not properly chosen. The paper starts by describing the optimization tool that was developed to solve the re-entry optimal control problem for a representative reusable SSTO and the uncertainty methodology. The succeeding section describes the various model subsystems used to evaluate the spaceplane performance. The specific trajectory optimization problem is then addressed, followed by a discussion of the results.

2. Optimization and robustness analysis

2.1 Trajectory optimization

All practical methods for solving an optimal control problem involve an approach in which the system is converted into a finite dimensional approximation. This methodology is known as the transcription method. The dynamic system, characterized by continuous functions, is converted into a problem of a finite set of variables: the resulting dimensional problem is then solved using a parameter optimization method. A further step aims to assess the accuracy of the finite dimensional approximation. This methodology allows one to re-write the optimal control problem into a non-linear programming problem (NLP). There are several methods that can be used to transcribe the optimal control problem into a NLP [2]. The single shooting method is the simplest technique to solve the NLP, where only the system controls are discretized and the whole optimization process iterates over the integration of dynamic system from initial to final conditions. The advantage of using a single shooting method is that the transcribed problem involves a small number of design variables; the disadvantage is that a small change in the initial condition compromises the boundary condition accuracy. A more sophisticated approach is the direct collocation method where both the controls and the state variables defining the system are discretized in terms of the elapsed time. In this way, an infinite-dimensional ODE system is replaced by a finite number of equality constraints, and the integrals associated with the objective and constraint functions of the original problem are approximated. This approach gives a large but sparse NLP, which can be solved conveniently using any one of a number of sequential quadratic programming (SQP) solvers [3] . The hybrid optimization technique adopted here is based on a mixed formulation which combines a population-based stochastic algorithm with a deterministic gradient-based method. Population-based stochastic algorithms are able to explore the global search space efficiently, and are able to find a feasible solution when the constraints are sufficiently loose and the number of the design variables is not too high (generally less than 100 variables). Deterministic gradient based solvers can deal efficiently with equality constraints and the high dimensionality of the typical problem. The hybrid method aims first to explore the control search space by using a stochastic approach coupled to a single shooting transcription method to evaluate the performance of candidate solutions, relaxing the system constraints and tolerances on the final states of the system. The second step involves a local optimization which aims to improve the value of the objective function and to ensure that strict equality constraints for the system are satisfied. A general overview of the optimization method that was used in this work is summarized in Fig. 1 and is described in detail below.

1. **Transcribe the optimal control problem into a single shooting NLP** The optimal control problem is converted to a non linear programming problem with a finite set of variables by using a single shooting method.

2. **Solve the single shooting NLP using MOPED** The single shooting NLP is then solved using an hybrid Evolutionary Algorithm (EA) which is obtained by coupling a Multi-Objective Parzen-based Estimation of Distribution [4] (MOPED) and a modified version of the Inflationary Differential Evolution Algorithm (IDEA) [5], [6]. The MOPED algorithm belongs to a subset of Evolutionary Algorithms called Estimation of Distribution Algorithms (EDA) [7]. These algorithms build a probabilistic model of the search space, and the evolutionary search operators, such as crossover and mutation, are replaced by a sampling procedure that operates on the probabilistic representation: the Parzen method [8] which builds a probabilistic representation of Pareto optimal solutions, with multivariate dependencies among variables [4]. The Parzen method uses a non-parametric approach to kernel density estimation which gives rise to an estimator that converges everywhere to the true Probability Density Function (PDF) in the mean square sense. Starting from the current population, the individuals are sampled from a uniform probability density function (PFDs) and then ranked by using NSGA-II techniques [9]: non-dominated sorting and crowding operators are used to classify promising solutions in the objective space. On the basis of information given by the individuals, the Parzen method allocates identical probability density function,

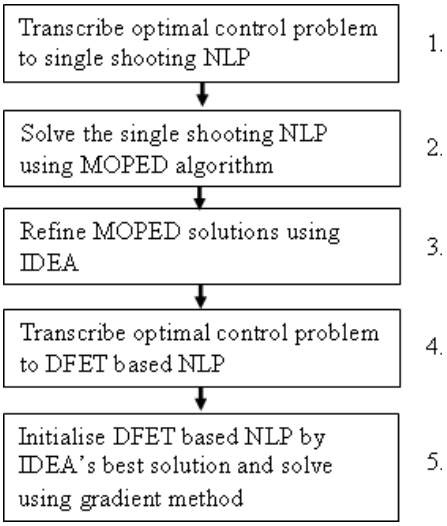

Figure 1: General scheme for the trajectory optimisation process.

each one centered on a different element of the sample. A probabilistic model of the promising search space is built on the statistical data provided by the individuals, and new individuals are sampled by the probabilistic model itself. Fitness values are used in order to evaluate the kernels variance and to favour sampling in the neighbourhood of the most promising solutions. MOPED explores the search space efficiently, but often prevents fine convergence on the optimal point, in particular when the solutions are spread over different areas of the feasible space. This feature led to the coupling of MOPED with IDEA, to give better convergence properties.

3. Refine MOPED solution using IDEA The Inflationary Differential Evolution Algorithm (IDEA) is based on a hybridization of a differential evolution (DE) variant [10] and the logic behind monotonic basin hopping (MBH) [11]. IDEA has been demonstrated to out-perform both DE and MBH on some difficult design problems, for instance those where the search space has a (multi) funnel-like structure [5] . The final solutions obtained by MOPED are clustered based on the Euclidean distance between them in the search space, resulting in a variable number of solutions clusters. For each of them, a threshold distance is chosen such that each cluster has a certain number of individuals. A DE mechanism is performed a number of times, beginning with the sub-population of each cluster. Each process is stopped only when the population contracts to below a predefined threshold. Every time the DE stops, a local search is performed in order to converge properly to the local optimum. Since the design optimisation in this case is constrained, the internal DE mechanism can be modified such that the comparison of individuals during the DE process is able to account for the constraints on the system before optimality in terms of the objective function for the system is assessed.

4. Transcribe the optimal control problem using DFET The optimal control problem is converted to a non linear problem programming using a direct transcription method based on Finite Elements in Time (DFET) on a spectral basis [12] .

5. Initialize DFET-based NLP using best solution from IDEA and solve using gradient method. The NLP problem is then solved by using a gradient-based optimization method, where the starting point is the solution obtained by the previous stochastic approach.

2.2 Robust design and uncertainties

Within the early stages of design, possible sources of uncertainties which affect the models need to be characterized to consider their impact on the design and to properly assess the performance of the system. Uncertainties occur across various phases of modeling and simulation, for instance the mathematical representation of the physical system, and its inherent variation. Two different types of uncertainties can be identified: (*a*) aleatory uncertainty arises from the fact that the system can have a random behaviour, (*b*) epistemic uncertainty results from a lack of knowledge about the system. Once the uncertainty levels have been estimated, it is possible to perform several different analyses, for instance: (*i*) an evaluation of the sensitivity of the nominal control law in the presence of the estimated uncertainties,

(*ii*) a statistical characterization of the vehicle performance in the presence of the uncertainties, (*iii*) a robust optimization of the trajectory, optimising the performance and minimising the effect of the uncertainties. In this paper an uncertainty model has been used to perform a robustness analysis of the nominal control law: once the optimal re-entry trajectory has been evaluated by using the nominal models, the optimal control law is reintegrated by using the perturbed outputs of the model subsystems. In the second analysis the uncertainties are implemented directly within the optimization loop, and the optimal performance of the vehicle is evaluated. Multiple optimizations are performed, each one adopting a different perturbed profile of the uncertain variable. In order to correctly assess the feasibility of the re-entry trajectory, a number of model parameters need to be considered as uncertain. Specifically here, the quantities affected by uncertainty are the atmospheric pressure and temperature, as they influence others parameters within the atmospheric model, such as the speed of sound and the density through the gas equation of state. By perturbing the atmospherics data, an uncertainty is generated within the aerodynamic model through its inputs, such as Mach number and dynamic pressure.

2.3 Uncertainties model

The perturbation of a specific variable is represented by a percent deviation around the nominal value of the uncertain system parameter; denoting the nominal quantity as x_{nom}, the uncertain value x_{unc} is defined as follows:

$$x_{unc} = x_{nom} + \varepsilon S_E x_{nom} \tag{1}$$

where ε is an error bound function which depends on the operational condition. S_E denotes a sampling surface which maps the set of operational conditions into the range [-1, 1], and the resulting interpolation depends on the values on each node. In order to perform a robustness analysis of the vehicle performance, n sets of values for the parameters defining S_E are randomly generated. For the robustness analysis of the nominal control law, the process generates n different S_E surfaces by randomly choosing the values defining S_E from an uniform distribution in the interval [-1; 1], where n is the total number of integrations performed. For the multiple optimization robustness analysis, the same set of n S_E surfaces are used to generate n optimised trajectories that account for the uncertainty in the system.

3. System models

This section presents the mathematical models used to simulate the vehicle performance during the re-entry, in particular, a description of aerodynamics, thermal model, atmosphere and dynamic model used to represent the vehicle behaviour during a descent profile starting at hypersonic regime and altitude of 120 km and ending at 24 km and at supersonic speed at the TAEM point.

3.1 Dynamic model

The vehicle is considered to be a point mass flying around a spherical and rotating Earth. The motion of the vehicle is governed by the following set of dynamic equations [13]:

$$\dot{h} = v sin\gamma \tag{2}$$

$$\dot{v} = -\frac{D}{m} - g\sin\gamma + \omega_e^2 (R_e + h)\cos\lambda(\sin\gamma\cos\lambda - \cos\gamma\sin\chi\sin\lambda) \tag{3}$$

$$\dot{\gamma} = \frac{L}{mv}\cos\mu - \left(\frac{g}{v} - \frac{v}{R_e + h}\right)\cos\gamma + 2\omega_e\cos\chi\cos\lambda + \omega_e^2\left(\frac{R_e + h}{v}\right)\cos\lambda\,(\sin\chi\sin\gamma\sin\lambda + \cos\gamma\cos\lambda) \tag{4}$$

$$\tag{5}$$

$$\dot{\chi} = \frac{L}{mv\cos\gamma}\sin\mu - \left(\frac{v}{R_e + h}\right)\cos\gamma\cos\chi\tan\lambda + 2\omega_e(\sin\chi\cos\lambda\tan\gamma - \sin\lambda) - \omega_e^2\left(\frac{R_e + h}{v\cos\gamma}\right)\cos\lambda\sin\gamma\cos\chi \tag{6}$$

$$\dot{\lambda} = \frac{v\cos\gamma\sin\chi}{R_e + h} \tag{7}$$

$$\dot{\theta} = \frac{v \cos\gamma cos\chi}{(R_e + h)\cos\lambda} \tag{8}$$

where h denotes the altitude above mean sea level, v is the magnitude of velocity in a rotating Earth-centered reference frame, γ indicates the flight path angle, χ is the path directional angle, μ is the bank angle, λ and θ denote respectively the latitude and the longitude, $m = 60000$ kg is the mass of the vehicle, L and D indicate aerodynamic lift and drag forces. $R_e = 6375$ km is the mean Earth radius, $\omega_e = 7.2921 \times 10^{-5} rad/s$ is the rotational velocity of the Earth and $g_0 = 9.80665\ m/s^2$ is the gravity acceleration at sea level. The control law governs the angle of attack and the bank angle, and these equations allow the vehicle's out of plane motion to be taken into account.

3.2 Thermal model

For the re-entry design process, the heat flux is assumed to be convective. The maximum heat flux to the vehicle is assumed to be adequately represented by a simple analytical model:

$$\dot{q}_{conv} = K_e \left(\frac{\rho}{R_n}\right)^{1/2} v^3 \tag{9}$$

where $k_e = 5.19111 \times 10^{-5} (kg/m^2)^{1/2}$, ρ is the atmospheric density and R_n is the radius of curvature of the stagnation area. The variation of the radius of curvature with the angle of attack for the vehicle studied in this paper has been calculated using the HyFlow software [14] for $\alpha \in [0, 85]$ deg, as reported in Fig. 2.

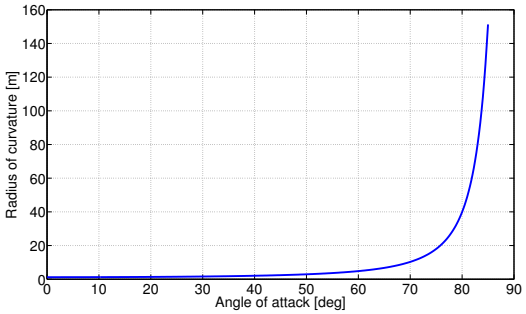

Figure 2: Radius of curvature as a function of angle of attack.

3.3 Earth model

The gravitational field is assumed to be a function of altitude and varies according to an inverse square law $g(h) = g_0(h/(Re + h))^2$. The atmospheric characteristics (temperature, pressure, density and speed of sound) follow the US Standard Atmosphere 1976 model up to 1000 km.

3.4 Aerodynamic model

The aerodynamic forces acting on the vehicle are function of the angle of attack α and flight Mach number M and are evaluated using a simple analytical model. In the hypersonic regime, the non linear lift variation with the angle of attack is represented by Newtonian theory [15] as

$$C_{L,hs} = 2\frac{A_{wing}}{A_{ref}} \sin^2\alpha \cos\alpha \tag{10}$$

where A_{wing} is the area of the lifting surfaces of the vehicle. As the flight Mach number decreases towards the supersonic regime, the lift on the vehicle is more accurately modelled through linearized aerodynamic theory so that

$$C_{L,ss} = \frac{C_{L\alpha}}{\sqrt{M^2 - 1}} \frac{A_{wing}}{A_{ref}} \sin\alpha \cos\alpha \tag{11}$$

and $C_{L\alpha}$ denotes a constant depending on the vehicle geometry. The overall variation of lift coefficient with Mach number is then modelled using the following equation:

$$C_L = \frac{C_{L,ss} + C_{L,hs}}{2} + \sqrt{C_{L,ss}^2 + C_{L,hs}^2} \tag{12}$$

The drag coefficient of the vehicle is evaluated as

$$C_D = C_{D0}(M) + C_L \tan\alpha \tag{13}$$

where the first term C_{D0}, a function of the Mach number, accounts for the wave, base, and viscous drag of the vehicle and the second term is the induced drag of its lifting surfaces. The overall lift and drag forces on the vehicle are then obtained by multiplying by the dynamic pressure $1/2\ \rho v^2$ and the vehicle reference area A_{ref}. Figure 3 shows the lift and drag coefficients as a function of Mach number and angle of attack.

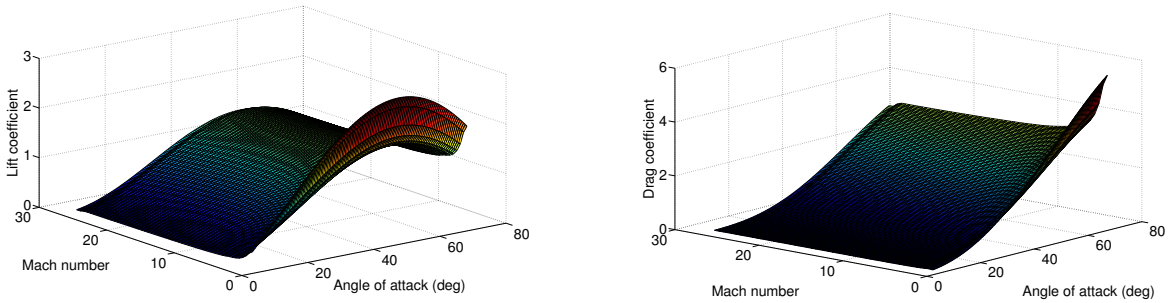

(a) Lift coefficient C_L versus Mach number and angle of attack (b) Drag coefficient C_D versus Mach number and angle of attack

Figure 3: Aerodynamics outputs for the SSTO vehicle.

4. Test case

For the re-entry trajectory problem, the control vector is given by $c = [\alpha, \mu, t]$, where t is the duration of the trajectory until the vehicle reaches the TAEM point. The search space D for the controls is defined by the following bounds: $\alpha \in [-10, 75]$ deg, $\beta \in [-80, 80]$ deg, and the flight time cannot exceed 3000 s. The bounds on the state vector are: $h \in [10, 180]$ km, $v \in [0.4, 9]$ km/s, $\gamma \in [-90, 90]$ deg, $\chi \in [-180, 180]$ deg, $\lambda \in [-180, 180]$ deg, $\theta \in [-180, 180]$ deg. The control law is the solution of the optimal control problem which aims to minimize the overall heat load acting on the vehicle:

$$\min_{\mathbf{c}\in D} \Big(q(t = t_f)\Big) \tag{14}$$

subject to the dynamics given by Eq. (2 - 8) . The initial point of the trajectory is defined as follows:

$$\begin{aligned} h(t=0) &= h_0 = 120 \text{ km} \\ v(t=0) &= v_0 = 7.8 \text{ km/s} \\ \gamma(t=0) &= \gamma_0 = -1 \text{ deg} \\ \chi(t=0) &= \chi_0 = 90 \text{ deg} \\ \lambda(t=0) &= \lambda_0 = 1 \text{ deg} \\ \theta(t=0) &= \theta_0 = 0 \text{ deg} \end{aligned} \tag{15}$$

The terminal conditions required at the TAEM phase are:

$$\begin{aligned} h(t=t_f) &= h_f = 24 \text{ km} \\ v(t=t_f) &= v_f = 0.8 \text{ km/s} \\ \gamma(t=t_f) &= \gamma_f = -10 \text{ deg} \\ \chi(t=t_f) &= \chi_f = 90 \text{ deg} \\ \lambda(t=t_f) &= \lambda_f = 40 \text{ deg} \\ \theta(t=t_f) &= \theta_f = 0 \text{ deg} \end{aligned} \tag{16}$$

Additional trajectory constraints are imposed on the heat flux so that $\dot{q} < 20000\ W/m^2$ and maximum normal acceleration $a_z < 28\ m/s^2$.

4.1 Shooting based evolutionary optimization

The evolutionary optimization scheme implements the shooting method to discretize the control law: the resulting control vector c is composed of a set of discrete control law values which are interpolated using a piecewise cubic interpolation and directly integrated in time. Within the control vector c, the angle of attack and bank angle are discretized into 17 elements each, $c(1:17) \in [-10, 75]$ deg, $c(18:34) \in [-10, 50]$ deg. The last design variable defines the duration of the trajectory, $c(35:36) \in [80, 3000]$ s. The equality constraints on final states are converted into inequality constraints such that $h_f \in [23, 25]$ km, $v_f \in [0.7, 0.9]$ km/s, $\gamma_f \in [-12, -8]$ deg, $\chi_f \in [89, 92]$ deg, $\theta_f \in [1, 1]$ deg and $\lambda_f \in [39, 41]$ deg.

4.2 Finite element in time direct collocation

The DFET method implemented in the optimisation process assesses the decomposition of the trajectory into N elements, each of which has n_p collocation points. The resulting set of non-linear algebraic equations obtained from the transcription method becomes the general non-linear programming problem (NLP) with the objective function:

$$\min_{\alpha_s, \delta_s, t_s} \Big(q(t = t_f) \Big) \tag{17}$$

subject to nonlinear algebraic constraints,

$$C(h_s, v_s, \gamma_s, \chi_s, \lambda_s, \theta_s, \alpha_s, \mu_s, t_s) = 0 \tag{18}$$

where h_s, v_s, γ_s, χ_s, λ_s, θ_s, α_s, μ_s denote NLP vectors containing the set of values of the state, control and time variable for each node defined by the DFET method. Due to the large number of variables involved, the NLP is solved by using a gradient-based deterministic algorithm.

4.3 Implementation of uncertainties

Generally the level of uncertainty in the atmospheric model increases with altitude. The US 1976 Standard Atmosphere used here is well known and identical to the Standard Atmosphere of the International Civil Aviation Organization up to 32 km; above this altitude, the US model becomes less accurate when compared to experimental data. Possible sources of uncertainty are the stochastic nature of the solar radiation absorbed and re-emitted by the Earth, which changes depending on geographical location. Further uncertainty can arise when creating a global atmospheric model, i.e. from the basic assumptions as to the average composition of air. For the atmospheric model, the uncertainty distribution function is defined as follows:

$$\varepsilon_{atm}(h) = l_{b,h}\left(1 - \frac{h}{h_c}\right) + u_{b,h}\left(\frac{h}{h_c}\right) \tag{19}$$

where $l_{b,h}$, $u_{b,h}$ indicate respectively the lower and the upper limits defined as percentage around the nominal value and increasing linearly the altitude, $h \in [h, h_c]$, and $h_c = 150$ km is a cut-off value, set equal to the maximum value of the altitude vector. The percentage boundaries for the atmospheric pressure are estimated as $u_{b,P} = 1$ %, $u_{l,P} = 30$ %, while the temperature boundaries are estimated as$u_{b,T} = 10$ %, $u_{l,T} = 30$ %. Fig. 4 shows an example of the approach applied to the temperature and compares the nominal profile with the perturbed temperature profile.

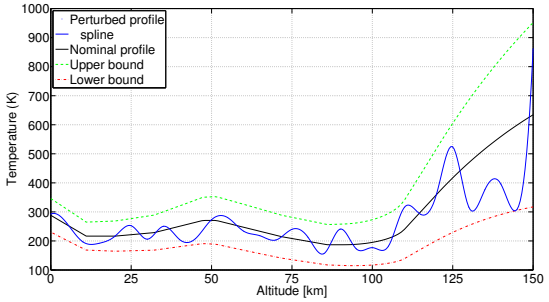

Figure 4: Nominal and perturbed values for the atmospheric temperature as a function of altitude.

5. Simulation results

Following the algorithm described in the previous section, a baseline trajectory is optimized using the nominal outputs from the system model. Figure 5 shows the optimized angle of attack α (see Fig.5a) and the bank angle μ (see Fig. 5b) as a function of time.

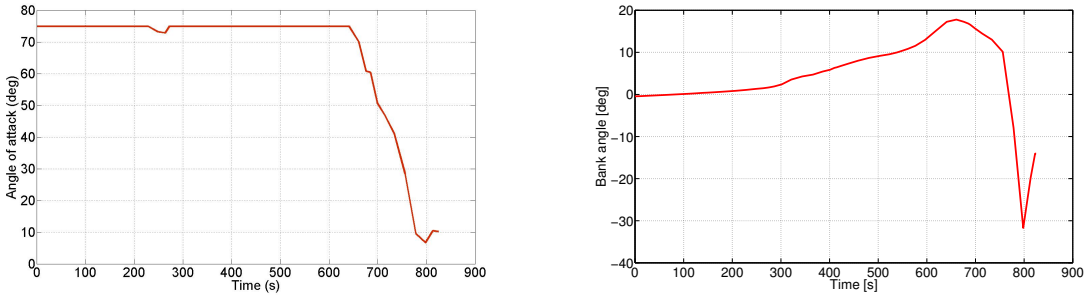

(a) Angle of attack (b) Bank angle

Figure 5: Nominal control laws for the re-entry trajectory.

The vehicle performs an initial atmosphere penetration phase at constant angle of attack of 75 deg: as the altitude decreases (see Fig. 6a) the heat flux increases (see Fig. 10b), reaching a local peak for a slightly decreased value of the angle of attack (Fig.5a) at about 263 s. A manoeuvre to increase the angle of attack follows to mantain the heat flux within the limit of 20000 W/m^2. The control law alters the bank angle of the vehicle to fulfil the final TAEM condition and to minimize the heat load on the vehicle. In order to analyze the sensitivity of the baseline control law to the model uncertainties, a set of 100 randomized atmospheric profiles were then implemented to perform 100 integrations of the control law shown in Fig. 5. The evolution of the state vector with time is shown in Fig. 6. As can be clearly seen none of the perturbed trajectories meets the target conditions (h=24 km, v=0.8 km/s, γ=-10 deg, χ=90 deg, θ=0 deg, λ=40 deg). Figure 7 and Table 1 report the statistics on the deviation of the perturbed trajectories from the target conditions. The full set of integrations converges towards the desired target conditions following a quasi-Gaussian distribution; Table 1 reports the mean value and standard deviation of final states: as can be seen, the mean values of the final state are lower than the target state. This first approach is helpful for a preliminary understanding of the robustness of the optimized control law.

Table 1: Statistics on the values of the design parameters

State	Mean	Standard deviation	Target values
Altitude, h (km)	23.803	0.6231	24
Velocity, v (km/s)	0.7634	0.0423	0.8
Flight path angle, γ (deg)	-9.9953	3.3489	-10
Directional path angle, χ (deg)	89.5942	1.791	90
Longitude, θ (deg)	-0.0015	0.0070	0
Latitude, λ (deg)	39.7746	0.2195	40

Since the perturbed trajectories do not fully satisfy the various path and final constraints, a more correct approach to evaluate the vehicle performance is to run 100 separate optimizations, each considering a different set of randomly perturbed system parameters. The resultant control laws are shown in Fig. 8. The control laws have the same pattern or shape as the nominal one, and are able to exactly meet the desired final conditions (see Fig. 9) whilst also fulfilling all the path constraints. Figure 10 shows the values of the normal acceleration and heat flux for the entire trajectory, demonstrating that the two constraints have been met.

The heat load computed from the set of 100 trajectories obtained using the optimized control laws can be statistically analysed. The mean value of the heat load along the re-entry trajectory is 7.5593 MJ/m^2 for the multiple optimization case, and the standard deviation is 74.323 kJ/m^2. Figure 12 shows the cumulative distribution functions (CDF) for the integration of the discrete PDF given in Fig. 11.

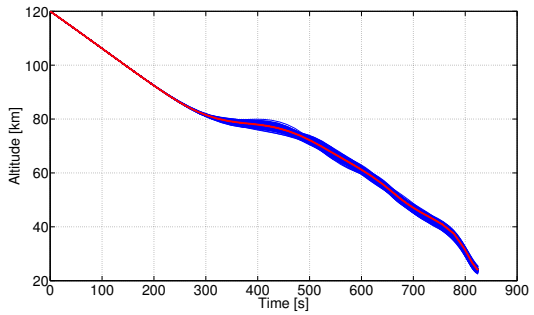

(a) Altitude

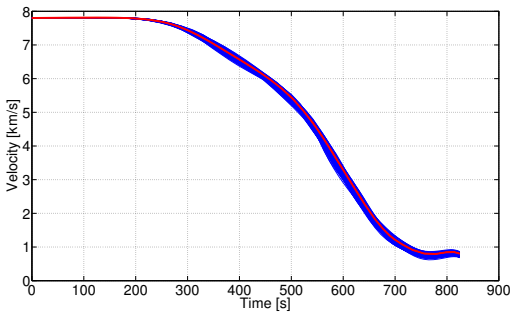

(b) Velocity

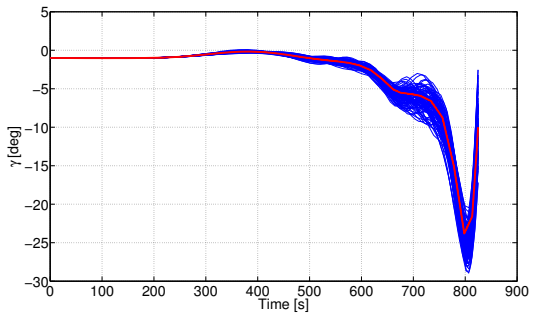

(c) Flight path angle

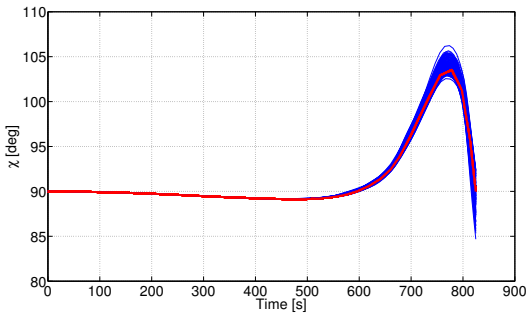

(d) Directional path angle

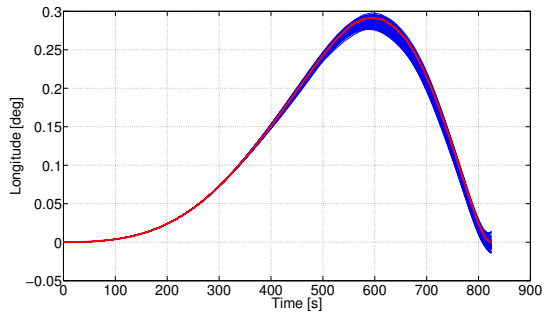

(e) Longitude

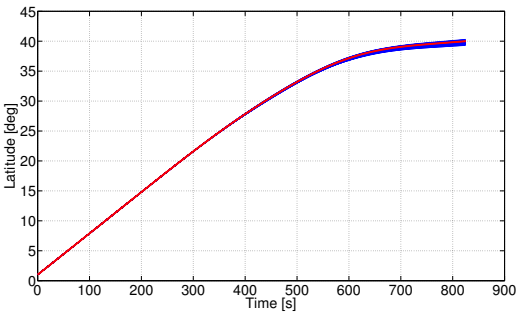

(f) Latitude

Figure 6: Evolution of the states, where the bold red lines refer to the nominal trajectory, and the blue lines refer to the integrated trajectories with perturbations present.

The information summarized in Fig. 12 can give an immediate understanding of the effect of uncertainties on the performance of the vehicle during the preliminary design phase, here shown in terms of the total heat load at the TAEM point. The upper right end of the curve corresponds to the worst case scenario, when the effect of the uncertainty has the largest negative impact, resulting a very high total heat load. On the other hand, the lower left end of the curve corresponds to the best case scenario, in other words the total heat load obtained when the effect of the uncertainty is the most favorable. The CDF curve gives the expectancy of obtaining a particular value of total heat load between the best and worst case values. If the uncertainties are correctly estimated, it can be guaranteed that in all cases the vehicle can arrive at the TAEM point with a total heat load which is equal to the worst case scenario (7.741 MJ/m^2), while there is a probability $p \leq 0.01$ that the vehicle will arrive to the final point with an amount of heat load equal to the value obtained in the best case scenario (7.422 MJ/m^2 in this case). It is therefore possible to have a direct quantification of the probability of a given final heat load value between the best case and the worst case values, e.g., a total heat load of 7.6108 MJ/m^2 can be obtained with $p = 0.8$, while a value of 7.501 MJ/m^2 can be obtained only with $p = 0.2$. It should be noted that while a sample size of only 100 is generally not considered large enough to draw accurate conclusions from the statistics, the sample size is large enough to test the validity and usefulness of this approach and to assess the potential for future work.

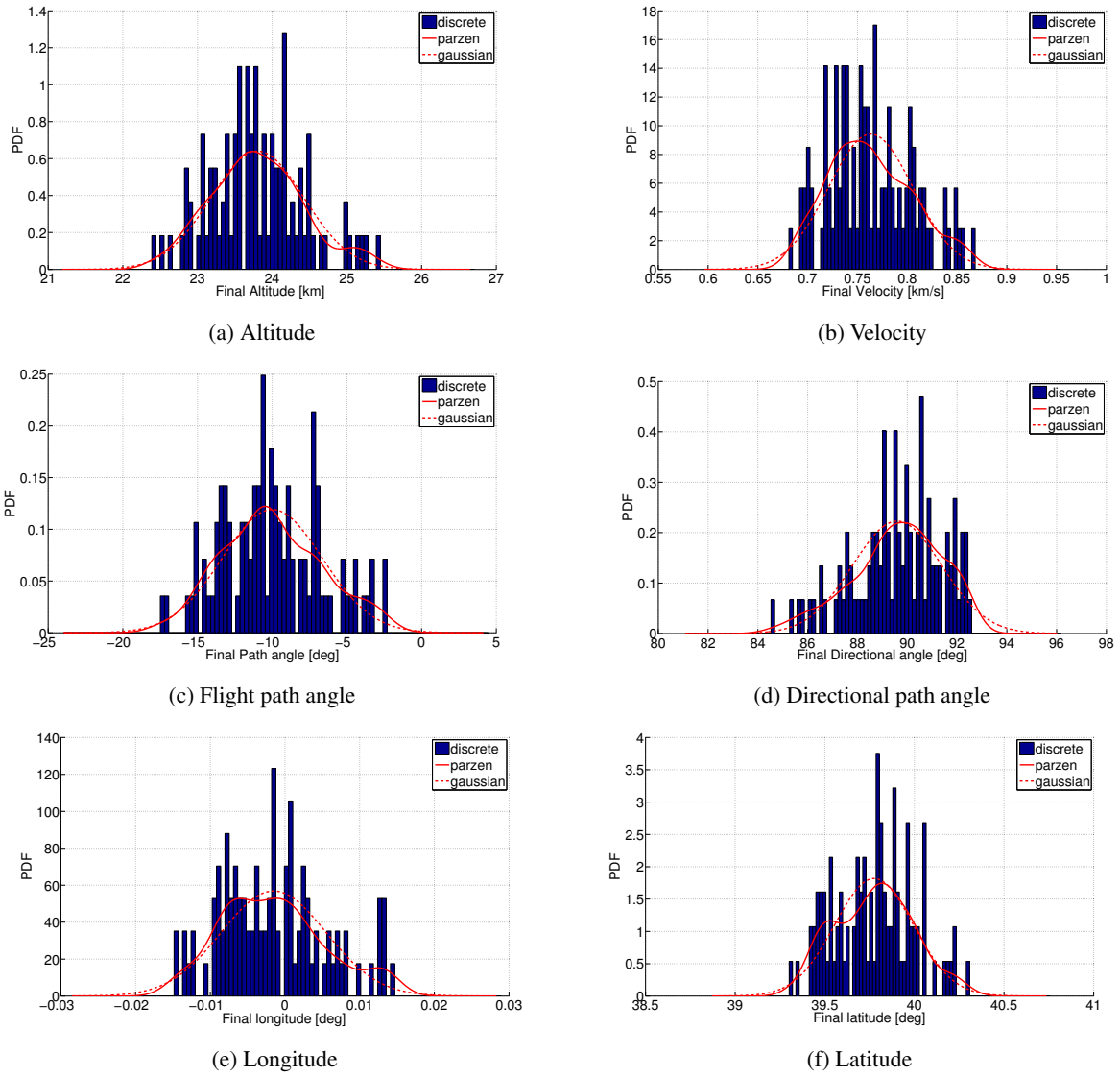

(a) Altitude

(b) Velocity

(c) Flight path angle

(d) Directional path angle

(e) Longitude

(f) Latitude

Figure 7: PDF of the final states when the nominal control laws are integrated using a perturbed atmospheric model.

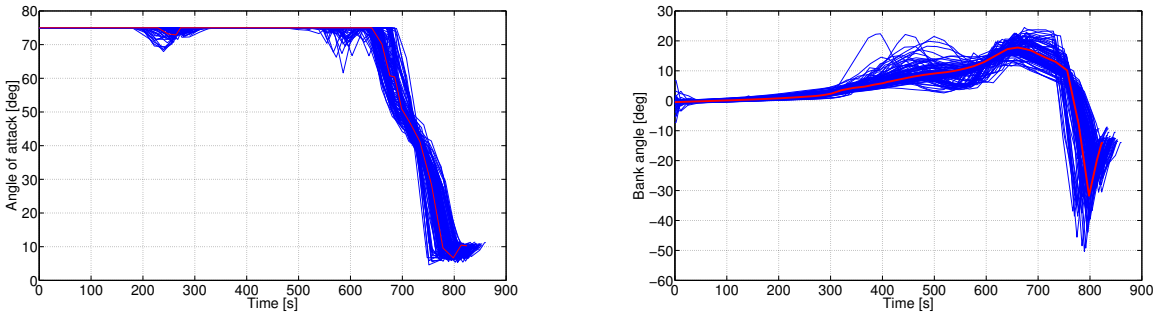

(a) Angle of attack

(b) Bank angle

Figure 8: Optimized control laws where the bold red lines refer to the nominal trajectory, and the blue lines refer to the integrated trajectory with perturbations present.

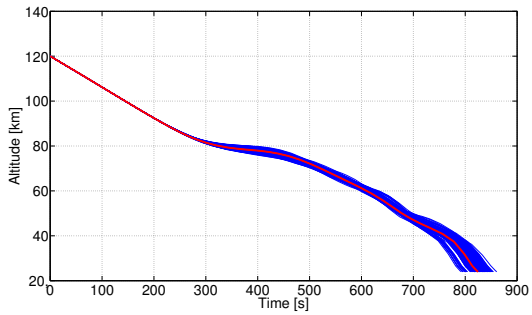

(a) Altitude

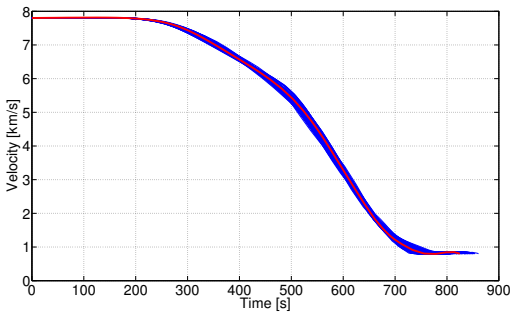

(b) Velocity

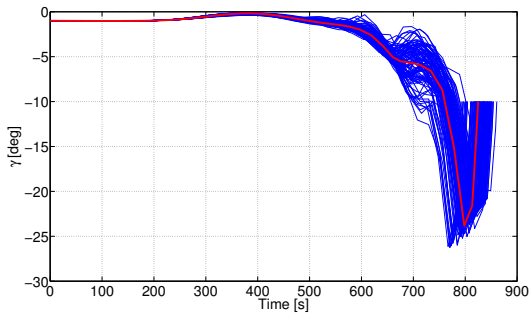

(c) Flight path angle

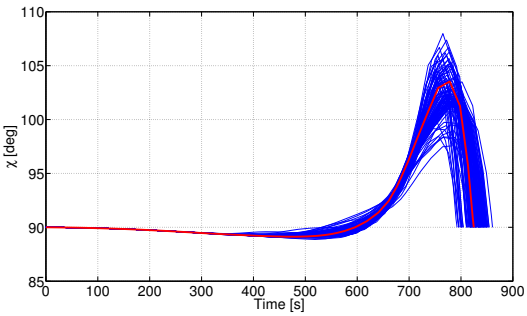

(d) Directional path angle

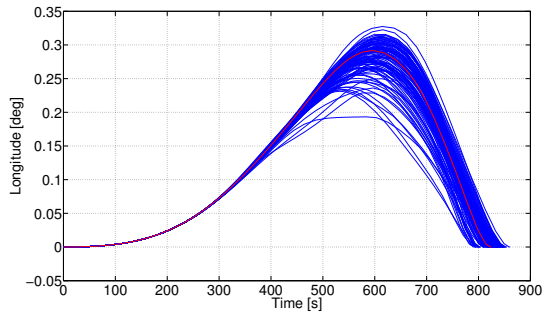

(e) Longitude

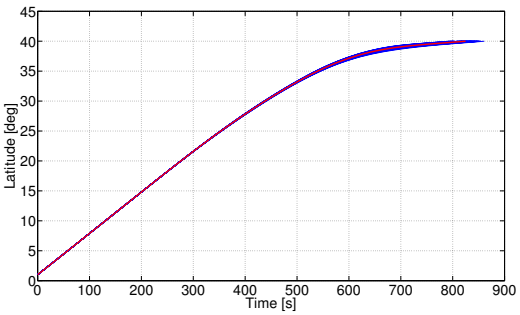

(f) Latitude

Figure 9: Evolution of the states for optimal control law where the bold red lines refer to the nominal trajectory, and the blue lines refer to optimised trajectories with perturbations present.

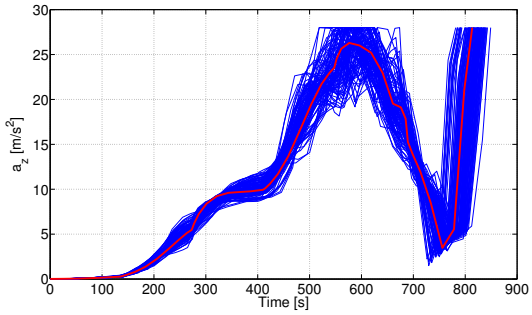

(a) Normal acceleration

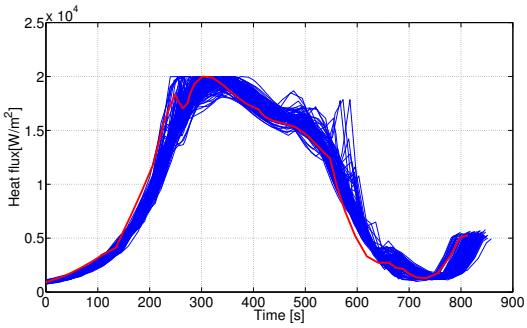

(b) Heat flux

Figure 10: Time evolution of the normal acceleration a_z and heat flux q, where the bold red lines refer to the nominal trajectory, and the blue lines refer to optimised trajectories with perturbations present.

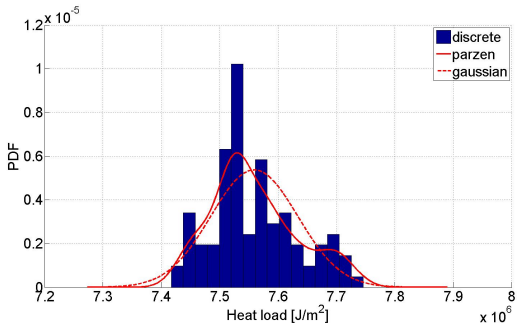

Figure 11: PDF of total heat load as obtained from the optimized trajectories.

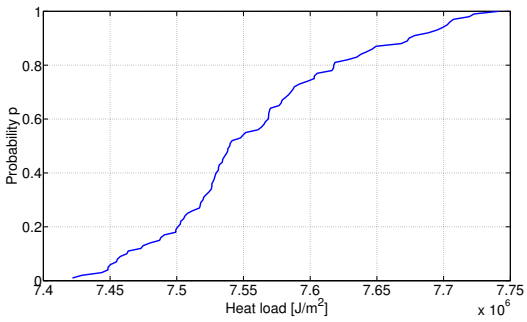

Figure 12: CDF curve of total heat load for the optimized trajectory

6. Conclusion

The paper describes a general approach for trans-atmospheric trajectory optimisation. A hybrid stochastic-deterministic algorithm and its application to the design of re-entry trajectory for an unpowered high performance, unmanned, single-stage-to-orbit vehicle as the last phase of a payload deployment into low Earth orbit has been detailed. Uncertainties in the atmospheric model have been considered, highlighting the need for the effect of epistemic and aleatory uncertainties to be considered from the very beginning of the design phase in order to have a proper estimation of the possible or probable performance of the vehicle. Integrating the trajectory using a static, nominal optimal control law with a randomly perturbed atmospheric model allows for a sensitivity analysis of the obtained control law, and allows the deviation of the results from the target final conditions to be evaluated. A second multiple optimisation approach is then performed, giving a performance expectancy curve based on the objective function, e.g., the total heat load, which can be used at the preliminary stage of the vehicle design to correctly estimate the performance of the vehicle accounting for uncertainties in the simulation models. Future work will aim towards the implementation of tools for the robust optimisation of trans-atmospheric trajectories, with the aim of optimising the expected values of performance while minimising the effect of uncertainties. The optimization analysis will be extended from the TAEM phase to account also for the landing approach of the SSTO vehicle. Future aerodynamic models will thus need to include a description of subsonic regime and a more realistic assessment of the uncertainties that are present within the aerodynamic model.

References

[1] De Ridder, S. and Mooij E. 2011. Optimal Longitudinal Trajectories for Reusable Space Vehicles in the Terminal area. In: *Journal of Spacecraft and Rockets*. Vol.48, No 4, Jul-August 2011.

[2] Betts, J. T. 2010. Practical Methods for Optimal control and Estimation using Nonlinear programming. Second edition, SIAM, 2010.

[3] Nocedal, J. and Wright, S. 2006. Numerical Optimization. Springer-Verlag Gmbh, 2nd ed., 2006.

[4] Costa, M. and Minisci, E. 2003. MOPED: a Multi-Objective Parzen-based Estimation of Distribution algorithm. In: *Second international Conference. EMO 2003*. edited by C. Fonseca, P. Fleming, E. Zitzler, K. Deb, and L. Thiele. Vol. 2632 of LNCS, Springer, Faro, Portugal, 08-11 April 2003.

[5] Vasile, M., Minisci, E. and Locatelli, M. 2011. An Inflationary Differential Evolution Algorithm for Space Trajectory Optimization. In: *IEEE Transactions on Evolutionary Computation*. Vol.15, No.2, 2011, pp.267-281.

[6] Minisci, E., Campobasso, M. S. and Vasile, M. 2012. Robust Aerodynamic Design of Variable Speed Wind Turbine Rotors. In: *ASME Turbo Expo 2*. Copenhagen, Denmark, June 11-15 2012.

[7] Lozano, J. A., Larranaga, P. and Inza, I. 2006. Towards a New Evolutionary Computation: Advances on Estimation of Distribution Algorithms (Studies in Fuzzness and Soft Computing). Springer, February 2006.

[8] Fukugana, K. 2012. Introduction to Statistical Pattern Recognition. Academic Press, 2012.

[9] Deb, K., Pratap, A., Agarwal, S. and Meyarivan, T. 2002. A Fast and Elitist Multiobjective Genetic Algorithm: NSGA-II. In: *IEEE Transactions on Evolutionary Computation*. Vol. 6, No.2, April 2002, pp182-197.

[10] Price, K., Storn, R., and Lampinen, J. 2005. Differential Evolution: a Practical Approach to Global Optimization. Springer, 2005.

[11] Leary, R. 2000. Global Optimization on Funneling Landscapes. In: *Journal of Global Optimization*. Vol. 18, No.4, 2000, pp367-383.

[12] Vasile, M. 2010. Finite Element in Time: a Direct Transcription Method for Optimal Control Problems. In: *AIAA/AAS Astrodynamics Specialist Conference*. AIAA Paper 2010-8275, Toronto, Canada, August 2-5 2010.

[13] Miele, A. M. 1990. Optimal Trajectories of Aircraft and Spacecraft. No.19910001655, JPL-956415, NAG1-516 in AGARD, Aircraft Trajectories: Computation, Prediction, Control, NASA, 1990.

[14] Wuilbercq, R., Ahmad, A., Scanlon, T. and Brown E R. Towards Robust Aero-Thermodynamic Predictions for Re-Usable Single-Stage to Orbit Vehicles. In: *18th AIAA/3AF International Space Planes and Hypersonic Systems and Technologies Conference*. Tours, France, September 24-28 2012.

[15] Anderson, J. D. editor. 2001. Fundamental of Aerodynamics. McGraw-Hill Higher Education, 3rd ed., 2001.